Inorganic Chemistry Communications 62 (2015) 11–14

Contents lists available at ScienceDirect

Inorganic Chemistry Communications

journal homepage: www.elsevier.com/locate/inoche

Short communication

A facile synthesis of water-soluble $BaYF_5$:Ln^{3+} NCs with excellent luminescent properties as promising contrast agent for dual-modal bioimaging

Cailing Chen [a], Chunguang Li [a,*], Liang Zhao [b], Xiaomin Liu [c], Tianyu Bai [a], He Huang [a], Zhan Shi [a,*], Shouhua Feng [a]

[a] State Key Laboratory of Inorganic Synthesis and Preparative Chemistry, College of Chemistry, Jilin University, Changchun 130012, PR China
[b] Department of Pathology, School of Stomatology, Jilin University, Changchun 130012, PR China
[c] State Key Laboratory of Luminescence and Applications, Changchun Institute of Optics, Fine Mechanics and Physics, Chinese Academy of Sciences, Changchun, 130012, PR China

ARTICLE INFO

Article history:
Received 18 August 2015
Received in revised form 12 October 2015
Accepted 13 October 2015
Available online 20 October 2015

Keywords:
Nanocrystals
Up-down conversion
Lanthanide
Bioimaging agent

ABSTRACT

Monodisperse, water-dispersible lanthanide (Ln^{3+})-doped $BaYF_5$ nanocrystals (NCs) are synthesized through a fast, facile and environmentally–friendly microwave-assisted modified polyol process with polyethyleneimine as the surfactant. The TEM images illustrate the sphere-like and flower-like morphologies of the obtained NCs. Intense multicolor down conversion (DC) luminescence is also achieved in Ce^{3+}/Ln^{3+} (Ln = Tb, Dy) doped $BaYF_5$ NCs. Then, upon excitation at 980 nm, upconversion (UC) luminescent properties of $BaYF_5$:Yb^{3+}/Ln^{3+} (Ln = Er, Tm, Ho) NCs and energy transfer between Yb^{3+} and Ln^{3+} are systematically surveyed. Furthermore, a layer of SiO_2 is coated on the surface of the NCs and the methyl thiazolyl tetrazolium (MTT) assays are performed to test the cytotoxicity of $BaYF_5$:Ln^{3+} NCs. Due to the X-ray absorption property of Ba element, a proof-of-concept CT imaging with $BaYF_5$:Ln^{3+} NCs is conducted. These results indicate that the obtained NCs have great potential as optical/CT bioprobe.

In recent years, biological imaging study has attracted considerable attention due to its ability of visualization [1]. There are many bioimaging techniques, such as fluorescent imaging and computed X-ray tomography (CT). These bioimaging techniques with their respective advantages play an important role in the clinical diagnosis and treatment. CT has high sensitivity for high density parts of the body rather than for soft tissue [2], whereas fluorescent imaging with higher sensitivity is suitable for cellular level imaging [3]. Therefore, the combination of CT and fluorescent imaging has the dual advantages of high sensitivity and high spatial resolution. Conventional fluorescent probes including semiconductor quantum dots and organic dyes are mostly excited by UV or short wavelength visible irradiation, but they also have some drawbacks, such as photobleaching, short lifetimes and potential toxicity to live cells [4,5]. As a result, exploring other alternatives is very urgent. Rare-earth fluorides can be an ideal choice due to their excellent photostability and low toxicity [6]. In particular, Ln^{3+}-doped upconversion (UC) fluorides have many advantages such as weak background autofluorescence, deep tissue penetration and large anti-Stokes shifts, thus have been widely used as bioprobes [7]. Up to now, the synthesis of Ln^{3+}-doped fluoride NCs is mainly based on the co-thermolysis method in non-hydrolytic solvents and hydrophobic NCs need complicated surface modification for further biological compatibility [8,9]. Because of the disadvantages of hydrophobic NCs, some groups have attempted to synthesize hydrophilic NCs [10,11]. Microwave-assisted synthesis is an important pathway due to its distinct strengths such as shorter reaction times, uniform heating and high yields [12,13]. Therefore, microwave-assisted solvothermal process can serve as an effective method to synthesize hydrophilic NCs. To our knowledge, Barium yttrium fluoride ($BaYF_5$) is considered to be a promising host matrix for luminescence and Ba element has large K-edge value and high X-ray mass absorption coefficient [14,15]. $BaYF_5$ NCs can be used as contrast agent for fluorescent imaging and CT imaging.

In this letter, we reported the synthesis of monodisperse, water-dispersible Ln^{3+}-doped $BaYF_5$ NCs through a fast, facile and environmentally–friendly microwave-assisted modified polyol process. A surfactant PEI was used to control the growth of the NCs and render the NCs dispersible in water. By adjusting the addition of Ln:F, the $BaYF_5$ NCs show two kinds of morphologies: sphere and flower. The up-down conversion luminescent properties of $BaYF_5$:Ln^{3+} NCs were systematically surveyed. In order to further explore their biological applications, a SiO_2 shell was coated on the NCs to improve the biocompatibility. MTT assays demonstrated that $BaYF_5$ NCs had low cytotoxicity. Furthermore, a proof-of-concept CT imaging with $BaYF_5$:Ln^{3+} NCs was conducted. These results suggest that the obtained NCs have great potential as optical/CT bioprobes.

* Corresponding authors.
E-mail address: cglee@jlu.edu.cn (C. Chen).

http://dx.doi.org/10.1016/j.inoche.2015.10.020
1387-7003/

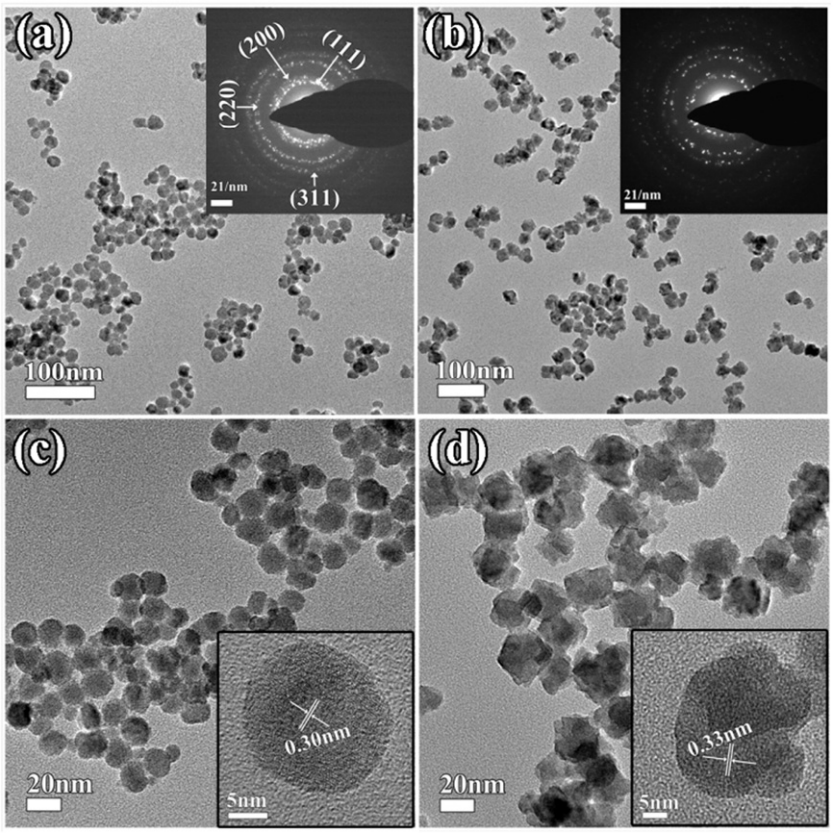

Fig. 1. TEM images, SAED patterns and HRTEM images of $BaYF_5$ nanospheres (a and c, inset of a and inset of c) and nanoflowers (b and d, inset of b and inset of d).

The size and morphology of the obtained $BaYF_5$ NCs can be tuned by simply modulating the ratio of Y^{3+}:F^- while keeping all other parameters fixed. Fig. 1 shows the TEM images of the as-synthesized $BaYF_5$ nanospheres and nanoflowers with average diameters of 16 and 29 nm (Fig. S1a), respectively. The pure nanospheres correspond to a ratio of Ln^{3+}:F^- of 1:5, whereas nanoflowers correspond to a ratio of Ln^{3+}:F^- of 1:4.2. The X-ray diffraction (XRD) patterns of $BaYF_5$ nanospheres and nanoflowers (Fig. S1b) are very similar. Comparison of tetragonal $BaYF_5$ (JCPDS:46-0039) with cubic $BaCeF_5$ (JCPDS:43-0394) shows that all diffraction peaks of the as-synthesized $BaYF_5$ NCs are well indexed to the latter except that the peak positions shift to larger angles due to the different radiuses between Ce^{3+} and Y^{3+}. These results are similar to some previous reports [15]. Lattice fringes are in agreement with the (111) planes and the selected area electron diffraction (SAED) patterns shown as insets of Fig. 1a and b confirm that the as-synthesized $BaYF_5$ NCs are cubic phase. Herein, we take $BaYF_5$ nanospheres as an example to analyze the structure and properties of the as-prepared NCs. Fig. 2 presents the XRD patterns of the as-synthesized $BaYF_5$ with different doping ions, which indicates that doping ions have no effect on product phase. As we can see from the XPS analysis (Fig. S1c), the oxidation states of the multivalent lanthanides are trivalent for the as-obtained Ln^{3+}-doped $BaYF_5$ up-down conversion NCs. The FT-IR spectrum (Fig. S1d) confirms that PEI is coordinated with the lanthanide ions.

$BaYF_5$ has been considered as an excellent matrix for optically active lanthanide ions. Fig. 3a shows the excitation and emission spectra of $BaYF_5$:15%Ce^{3+}/(5–15%)Tb^{3+} NCs in aqueous solution. The excitation spectra were recorded at the 544 nm emission ($^5D_4 \rightarrow {}^7F_5$) of Tb^{3+}, corresponding to the absorption of the 4f–5d band of Ce^{3+}. The weak emission of Ce^{3+} (300–400 nm, Fig. S2a) and strong emission of Tb^{3+} (450–650 nm) caused by transitions between the excited $^5D_4$ state and the ^7F_J (J = 6–3) ground states of the Tb^{3+} ions indicate an energy transfer from Ce^{3+} to the Tb^{3+} ions, as shown in Fig. 3d. The emission intensity increases with the higher doping concentration of Tb^{3+} from 5% to 15%, and it is obvious that the emission intensity of $BaYF_5$:Ce^{3+}/Tb^{3+} NCs is affected by the concentration of Tb^{3+} ions. Detailed photoluminescence studies were also carried out on $BaYF_5$ doped with varying concentrations of Dy^{3+} ions (Fig. 3b). Unlike $BaYF_5$:Ce^{3+}/Tb^{3+} samples, the emission intensity decreases with increasing Dy^{3+} concentration, which can be explained based on concentration quenching due to crossrelaxation among Dy^{3+} ions. The luminescence decay curve of Tb^{3+} in $BaYF_5$:15%Ce^{3+}/15%Tb^{3+} and Dy^{3+} in $BaYF_5$:15%Ce^{3+}/5%Dy^{3+} NCs in an aqueous solution is shown in Fig. S2b and c, respectively. And the corresponding calculated CIE coordinates are shown in Fig. 3c. Furthermore, we have tested the absolute luminescence quantum yields (QYs), which have shown that QYs of

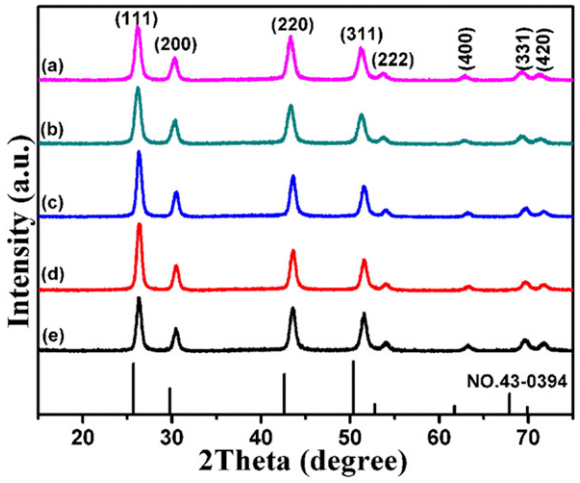

Fig. 2. XRD patterns of (a) $BaYF_5$:Ce^{3+}/Tb^{3+}, (b) $BaYF_5$:Ce^{3+}/Dy^{3+}, (c) $BaYF_5$:Yb^{3+}/Er^{3+}, (d) $BaYF_5$:Yb^{3+}/Tm^{3+}, (e) $BaYF_5$:Yb^{3+}/Ho^{3+} nanocrystals.

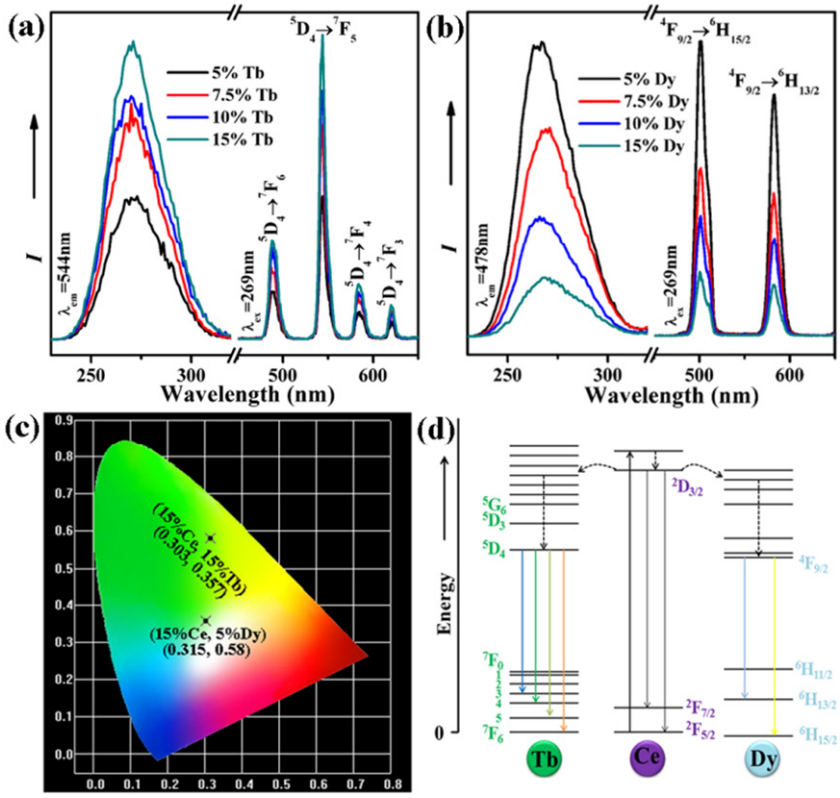

Fig. 3. Excitation and emission spectra of (a) $BaYF_5:Ce^{3+}/Tb^{3+}$ and (b) $BaYF_5:Ce^{3+}/Dy^{3+}$ NCs; (c) Corresponding calculated CIE coordinate diagram of optimal emission of $BaYF_5$: Ce^{3+}/Ln^{3+} NCs; (d) Proposed energy transfer mechanisms between Ce^{3+} and Ln^{3+} in the $BaYF_5:Ce^{3+}/Ln^{3+}$ NCs.

$BaYF_5$:15%Ce^{3+}/15%Tb^{3+} and $BaYF_5$:15%Ce^{3+}/5%Dy^{3+} NCs are 22.50% and 9.92%, respectively. In the procedure of testing, the aberration inevitably appears in the QY due to miscellaneous factors.

Owing to high fluorescence efficiency, ease of dispersion and small feature size, these $BaYF_5:Ln^{3+}$ NCs can readily be embedded in polydimethylsiloxane (PDMS) monoliths to construct 3D color displays,

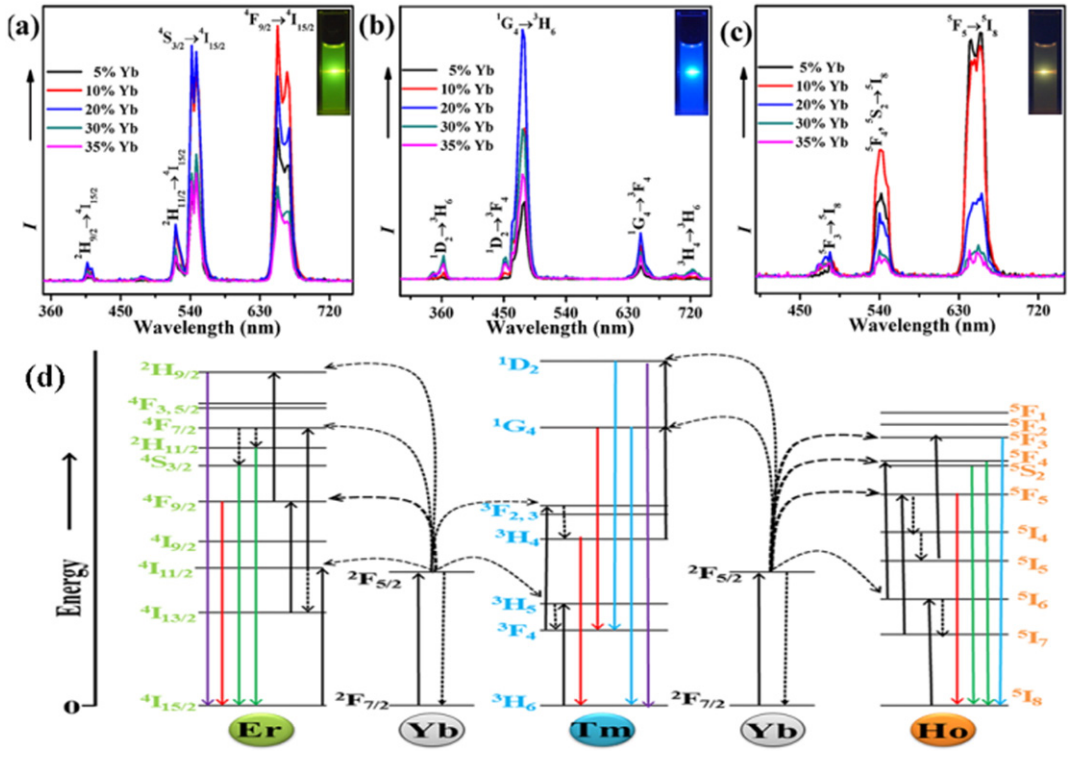

Fig. 4. UC emission spectra of (a) $BaYF_5:Yb^{3+}/Er^{3+}$, (b) $BaYF_5:Yb^{3+}/Tm^{3+}$ and (c) $BaYF_5:Yb^{3+}/Ho^{3+}$ upon excitation at 980 nm, (inset: the corresponding luminescence photographs of the samples with optimal emission under 980 nm irradiation); (d) proposed energy transfer mechanisms between Yb^{3+} and Ln^{3+} in the $BaYF_5:Yb^{3+}/Ln^{3+}$ NCs.

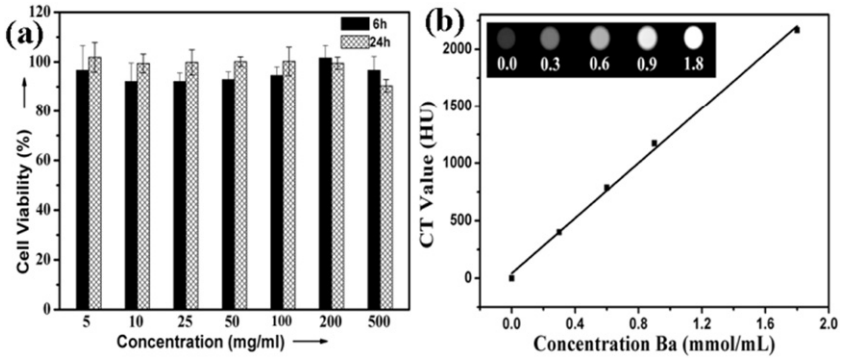

Fig. 5. (a) Cell viability of HeLa cells after incubation with $BaYF_5$ NCs for 6 h and 24 h; (b) CT value (HU) for the different Ba^{2+} concentrations of $BaYF_5$ NCs, Inset: corresponding CT images in aqueous solutions.

presenting beautiful colors. Fig. S2d demonstrates that the composites containing $BaYF_5$:Ce^{3+}/Tb^{3+} NCs is white under sunlight and green under UV irradiation.

The UC properties of $BaYF_5$:Ln^{3+} NCs have also been investigated. Fig. 4a–c shows the UC fluorescence spectra of the $BaYF_5$:(5–35%)Yb^{3+}/(2%)Ln^{3+} (Ln = Er, Tm, Ho) NCs. As shown in Fig. 5a, UC intensity first increases and then decreases with the increasing doping concentration of Yb^{3+}. The maximum UC intensity at 654 nm occurs when the doping concentration of Yb^{3+} is 10%, but the maximum value at 540 nm is achieved under the 20% Yb^{3+} doping, which results can be explained by Fig. 4d. From the proposed energy transfer mechanisms, $^4S_{3/2} \rightarrow {}^4I_{15/2}$, and $^4F_{9/2} \rightarrow {}^4I_{15/2}$ transitions are both two-photon process. For $^4F_{9/2} \rightarrow {}^4I_{15/2}$ transition, there is a non-radiative relaxation process and this process extend the waiting time of the next photon coming, which can be achieved at the lower doping concentration of Yb^{3+}. However, for $^4S_{3/2} \rightarrow {}^4I_{15/2}$ transition, Er^{3+} continuously absorbs two photons passed from Yb^{3+}, and the higher concentration of Yb^{3+} must be acquired to achieve the maximum. When the Yb^{3+} doping concentration is too high, concentration quenching will occur. For the NCs with Tm^{3+}, the UC intensities increase when the doping concentration of Yb^{3+} increases from 5% to 20%, but the concentration quenching occurs if Yb^{3+} concentration goes higher. The Ho^{3+}-doped NCs have similar results with Er^{3+}-doped. At 654 nm, the maximum UC intensity occurs if the doping concentration of Yb^{3+} is 5%, but at 540 nm, the maximum value is achieved under the 10% Yb^{3+}. For $^5F_5 \rightarrow {}^5I_8$ and $^5S_2 \rightarrow {}^5I_8$ transitions, they are both two-photon processes, but there is a non-radiative relaxation process ($^5I_6 \rightarrow {}^5I_7$) in the process of $^5I_8 \rightarrow {}^5F_5$.

A thin silica surface modification was required to improve biocompatibility and conjugate biomolecules. As seen from Fig. S3, a core/shell structure is obtained by coating silica on $BaYF_5$:Ln^{3+} NCs. We used MTT assay to test the cytotoxicity. As shown in Fig. 5a, upon incubating the HeLa cells with even 500 μg/ml $BaYF_5$:Ln^{3+} NCs, more than 90% of the cells were alive after 24 h of exposure, which suggest that the $BaYF_5$:Ln^{3+} NCs have excellent biological compatibility and could be a promising candidate as bioprobe. Due to the high X-ray absorption coefficient of Ba element, the $BaYF_5$:Ln^{3+} NCs should have the potential as promising nanoparticle-based CT contrast agents. Fig. 5b shows a good linear correlation between the X-ray adsorption, so called Hounseld unit (HU) value, and the concentrations of $BaYF_5$:Ln^{3+} NCs in water at X-ray energies of 120 kV. As shown in the inset of Fig. 5b, the intensities of CT images enhanced with the increasing concentration of $BaYF_5$:Ln^{3+} NCs. This encouraging result indicates the feasibility of the $BaYF_5$ NCs as CT contrast agent.

In summary, we have synthesized monodisperse, water-dispersible Ln^{3+}-doped $BaYF_5$ NCs with two kinds of morphologies: sphere and flower, by a fast, facile and environmentally-friendly microwave-assisted modified polyol process. The up–down conversion fluorescent properties have been investigated in detail. To further explore the biological applications, a layer of SiO_2 was coated on the surface of the NCs and MTT assays were performed to test the cytotoxicity of $BaYF_5$:Ln^{3+} NCs, which demonstrates that these NCs have low toxicity and biocompatibility. Moreover, a proof-of-concept application was conducted by taking $BaYF_5$:Ln^{3+} NCs as CT imaging agent. All above, as-prepared Ln^{3+}-doped $BaYF_5$ NCs have great potential as optical/CT dual modal bioprobes.

Acknowledgments

This work was supported by the Foundation of the Natural Science Foundation of China (no. 21371069 and 21301068) and National High Technology Research and Development Program (863 program) of China (no. 2013AA031702).

Appendix A. Supplementary data

Supplementary data to this article can be found online at http://dx.doi.org/10.1016/j.inoche.2015.10.020.

References

[1] J. Rieffel, F. Chen, J. Kim, G. Chen, W. Shao, S. Shao, et al., Adv. Mater. 27 (2015) 1785–1790.
[2] Z. Liu, E. Ju, J. Liu, Y. Du, Z. Li, Q. Yuan, et al., Biomaterials 34 (2013) 7444–7452.
[3] Q. Liu, M. Chen, Y. Sun, G. Chen, T. Yang, Y. Gao, et al., Biomaterials 32 (2011) 8243–8253.
[4] S. Kim, T.Y. Ohulchanskyy, H.E. Pudavar, R.K. Pandey, P.N. Prasad, J. Am. Chem. Soc. 129 (2007) 2669–2675.
[5] S. Han, L. Hu, N. Gao, A.A. Al-Ghamdi, X. Fang, Adv. Funct. Mater. 24 (2014) 3725–3733.
[6] Y. Liu, D. Tu, H. Zhu, R. Li, W. Luo, X. Chen, Adv. Mater. 22 (2010) 3266–3271.
[7] G. Tian, Z. Gu, L. Zhou, W. Yin, X. Liu, L. Yan, et al., Adv. Mater. 24 (2012) 1226–1231.
[8] X. Wang, J. Zhuang, Q. Peng, Y. Li, Nature 437 (2005) 121–124.
[9] F. Wang, Y. Han, C.S. Lim, Y. Lu, J. Wang, J. Xu, et al., Nature 463 (2010) 1061–1065.
[10] F. Li, C. Li, X. Liu, Y. Chen, T. Bai, L. Wang, et al., Chem. Eur. J. 18 (2012) 11641–11646.
[11] Y. Huang, H. You, G. Jia, Y. Song, Y. Zheng, M. Yang, et al., J. Phys. Chem. C 114 (2010) 18051–18058.
[12] H.Q. Wang, T. Nann, ACS Nano 3 (2009) 3804–3808.
[13] C. Chen, L.D. Sun, Z.X. Li, L.L. Li, J. Zhang, Y.W. Zhang, et al., Langmuir 26 (2010) 8797–8803.
[14] C. Zhang, P.A. Ma, C. Li, G. Li, S. Huang, D. Yang, et al., J. Math. Chem. 21 (2011) 717–723.
[15] H. Liu, W. Lu, H. Wang, L. Rao, Z. Yi, S. Zeng, et al., Nanoscale 5 (2013) 6023–6029.